J. Fluid Mech. (2025), *vol.* 1016, A3, doi:10.1017/jfm.2025.10384

JFM PAPERS

Beyond Nusselt number: assessing Reynolds and length scalings in rotating convection under stress-free boundary conditions

Veeraraghavan Kannan[1], **Jiaxing Song**[1,2], **Olga Shishkina**[2] and **Xiaojue Zhu**[1]

[1]Max Planck Institute for Solar System Research, Göttingen 37077, Germany

[2]Max Planck Institute for Dynamics and Self-Organization, Göttingen 37077, Germany

Corresponding author: Xiaojue Zhu, zhux@mps.mpg.de

(Received 19 March 2025; revised 27 May 2025; accepted 17 June 2025)

Convection in planetary environments is often modelled using stress-free boundary conditions, with diffusion-free geostrophic turbulence scalings frequently assumed. However, key questions remain about whether rotating convection with stress-free boundary conditions truly achieves the diffusion-free geostrophic turbulence regime. Here, we investigated the scaling behaviours of the Nusselt number (Nu), Reynolds number (Re) and dimensionless convective length scale (ℓ/H, where H is the height of the domain) in rotating Rayleigh–Bénard convection under stress-free boundary conditions within a Boussinesq framework. Using direct numerical simulation data for Ekman number Ek down to 5×10^{-8}, Rayleigh number Ra up to 5×10^{12}, and Prandtl number $Pr = 1$, we show that the diffusion-free scaling of the heat transfer $Nu - 1 \sim Ra^{3/2}\, Pr^{-1/2}\, Ek^2$ alone does not necessarily imply that the flow is in a geostrophic turbulence regime. Under the stress-free conditions, Re and ℓ/H deviate from the diffusion-free scalings, indicating a dependence on molecular diffusivity. We propose new non-diffusion-free scaling relations for this diffusion-free heat transfer regime with stress-free boundary conditions: $\ell/H \sim Ra^{1/8}\, Pr^{-1/8}\, Ek^{1/2}$ and $Re \sim Ra^{11/8}\, Pr^{-11/8}\, Ek^{3/2}$. Our findings highlight the need to assess both thermal and dynamic characteristics to confirm geostrophic turbulence.

Key words: Bénard convection, rotating flows

1. Introduction

Rotating thermal convection is a fundamental process observed in nature, occurring in the fluid cores of stars and planets, as well as in planetary atmospheres and oceans

(Atkinson & Zhang 1996; Marshall & Schott 1999; Aurnou *et al.* 2015). Understanding the dynamics of this process is crucial in geophysical and astrophysical contexts, where heat and momentum transport under rotational constraints sustain magnetic fields and drive large-scale flow structures (Heimpel, Gastine & Wicht 2016; Schumacher & Sreenivasan 2020). Among rotating thermal convection models, the rotating Rayleigh–Bénard convection (RRBC) framework provides valuable insights into rotation-influenced buoyancy-driven flows (Kunnen 2021; Ecke & Shishkina 2023).

In RRBC, a fluid layer is heated from below and cooled from above while rotating about a vertical axis. The heat transfer and flow properties in this system are described by key dimensionless parameters: the Rayleigh number (Ra), quantifying thermal driving; the Prandtl number (Pr), characterising fluid diffusivity; and the Ekman number (Ek), which measures rotational influence. In strongly rotational systems ($Ek \leq 10^{-4}$), increasing Ra leads to distinct convection regimes, ranging from rotation-dominated to buoyancy-dominated flows, each governed by unique scaling laws for heat and momentum transport (Julien *et al.* 2012*b*; Cheng *et al.* 2015; Aurnou, Horn & Julien 2020; Kunnen 2021; Ecke & Shishkina 2023). A well-known diffusion-free scaling law for heat transfer, $Nu - 1 \sim Ra^{3/2}\, Ek^2\, Pr^{-1/2}$, where Nu is the Nusselt number representing the ratio of total to conductive heat transfer, assumes independence from viscosity (ν) and thermal diffusivity (κ) (Stevenson 1979; Julien *et al.* 2012*a*; Stellmach *et al.* 2014; Cheng & Aurnou 2016; Plumley *et al.* 2017; Bouillaut *et al.* 2021; Song *et al.* 2024*c*; van Kan *et al.* 2025).

This diffusion-free heat transfer scaling is thought to represent an idealised geostrophic turbulence regime, where the system is independent of ν and κ, consistent with the energy cascade paradigm in high-Ra turbulent flows (Ahlers, Grossmann & Lohse 2009; Lohse & Shishkina 2024). Geostrophic turbulence, often termed ultimate Rayleigh–Bénard turbulence under strong rotation, is crucial for geophysical and astrophysical systems, such as planetary cores, atmospheres and stellar convection zones, where large Ra values occur (Vallis 2017). Understanding this regime is vital for predicting heat and mass transport in these environments. Despite recent advances in achieving ultimate turbulent scaling through direct numerical simulations (DNS) and experiments with taller convection cells (Cheng *et al.* 2018; Ecke & Shishkina 2023), replicating extreme conditions ($Ek \sim 10^{-7}$, $Ra \sim 10^{12}$) in laboratory experiments remains challenging. Only very recently, the diffusion-free heat transfer scaling has been observed with no-slip boundaries at very high Ra ($Ra > 10^{12}$) and very strong rotation ($Ek < 10^{-8}$) in DNS (Song *et al.* 2024*a*,*b*,*c*). In contrast, DNS studies and reduced asymptotic models suggest that stress-free boundaries are generally perceived as more favourable for achieving diffusion-free heat transfer. Diffusion-free scaling of Nu has indeed been observed at moderate Ekman numbers ($Ek < 10^{-6}$) (Julien *et al.* 2012*a*; Stellmach *et al.* 2014; Plumley & Julien 2019; Oliver *et al.* 2023; van Kan *et al.* 2025), significantly higher than thresholds for no-slip boundaries, leading researchers to believe that stress-free conditions more readily facilitate the exploration of the geostrophic turbulence regime.

The Nusselt number has traditionally served as the primary diagnostic for identifying diffusion-free scaling and geostrophic turbulence in rapidly RRBC (Stellmach *et al.* 2014; Bouillaut *et al.* 2021; Maffei *et al.* 2021; Oliver *et al.* 2023; Song *et al.* 2024*c*; van Kan *et al.* 2025). However, using no-slip boundary conditions, recent analyses suggest that relying solely on Nu scaling may be insufficient to fully capture the transition into the geostrophic turbulence regime (Song *et al.* 2024*c*). Achieving a truly diffusion-free state demands not only asymptotic thermal transport but also diffusion-free momentum transport, characterised by the Reynolds number (Re) and diffusion-free convective length scales (ℓ/H), normalised by the container height (H). Theoretical predictions for geostrophic turbulence anticipate clear, diffusion-independent scaling laws: $Re \sim Ra\,Ek\,Pr^{-1}$ and $\ell/H \sim Ra^{1/2}\,Ek\,Pr^{-1/2}$ (Guervilly, Cardin & Schaeffer 2019; Madonia *et al.* 2021; Oliver *et al.* 2023; Song *et al.* 2024*c*).

Stress-free boundary conditions are employed extensively in studies of planetary atmospheres, including Jupiter's (Christensen 2010; Fuentes *et al.* 2023), and solar convection dynamics (Featherstone & Hindman 2016; Vasil, Julien & Featherstone 2021; Käpylä 2024), under the implicit assumption that they naturally facilitate diffusion-free turbulence across thermal, momentum and structural measures. However, through our extensive DNS studies of idealised RRBC, we uncover a crucial and unexpected distinction. While Nu robustly transitions to diffusion-independent scaling at moderate Ek accessible to current simulations, Re and ℓ/H persistently exhibit significant residual dependence on viscosity. This divergence indicates that even as heat transport becomes effectively diffusion-free, viscous effects continue to influence the strength of convective motions and maintain larger-scale, viscosity-dominated coherent vortices in stress-free RRBC.

We therefore argue that genuine geostrophic turbulence can be unambiguously recognised only when Nu, Re and ℓ/H simultaneously exhibit diffusion-free scaling. Our extensive DNS datasets with stress-free boundary conditions, covering a wide parameter space with Ra and Ekman numbers down to $Ek = 5 \times 10^{-8}$, clearly show that the asymptotic, diffusion-free regime for Nu is achieved far in advance of Re and ℓ/H. This highlights a significant physical implication: current geophysical and astrophysical models employing stress-free boundaries with moderate Ek may underestimate the influence of viscosity on large-scale flow structures. Recent asymptotic theories, rescaled specifically for stress-free RRBC, propose that fully diffusion-free conditions across all diagnostics might require extremely low $Ek \sim 10^{-10}$ (van Kan *et al.* 2025). Exploring this parameter regime remains a formidable computational and experimental challenge, underscoring the need for innovative numerical techniques and novel experimental approaches to conclusively achieve and characterise the regime of fully developed geostrophic turbulence.

2. Numerical methods

In this study, we investigate RRBC by analysing DNS datasets from our recent work, utilising both stress-free and no-slip boundary conditions on the horizontal plates that bound the fluid domain. Specifically, we employ stress-free RRBC DNS data from Kannan & Zhu (2025), and no-slip RRBC simulation datasets from Song *et al.* (2024*a*,*b*,*c*) to conduct a detailed comparison of the geostrophic turbulence regime under these distinct boundary conditions, assuming fixed-temperature conditions on the horizontal plates, and periodic lateral boundaries in both cases. The Boussinesq approximation is applied to model the system, which rotates with constant angular velocity Ω around the vertical z-axis, with gravitational acceleration $\boldsymbol{g} = -g\boldsymbol{e}_z$, where $\boldsymbol{e}_z$ is the vertical unit vector.

The simulations were performed using the second-order finite-difference code AFiD (Verzicco & Orlandi 1996; van der Poel *et al.* 2015; Zhu *et al.* 2018). The reference scales adopted are the domain height H, the temperature difference between the plates Δ, and the characteristic free-fall velocity $u_f = \sqrt{\alpha_T g H \Delta}$, where α_T is the thermal expansion coefficient, and g is the gravitational acceleration. The dimensionless governing equations are

$$\nabla \cdot \boldsymbol{u} = 0, \tag{2.1}$$

$$\frac{\partial \boldsymbol{u}}{\partial t} + \boldsymbol{u} \cdot \nabla \boldsymbol{u} = -\nabla p + \sqrt{\frac{Pr}{Ra}}\, \nabla^2 \boldsymbol{u} + \theta \boldsymbol{e}_z - \frac{1}{Ek}\sqrt{\frac{Pr}{Ra}}\, \boldsymbol{e}_z \times \boldsymbol{u}, \tag{2.2}$$

$$\frac{\partial \theta}{\partial t} + \boldsymbol{u} \cdot \nabla \theta = \frac{1}{\sqrt{Ra\, Pr}}\, \nabla^2 \theta, \tag{2.3}$$

where $\boldsymbol{u}$ is the velocity field, p is the pressure, and T is the temperature.

The dimensionless control parameters are defined as

$$\Gamma = \frac{L}{H}, \quad Pr = \frac{\nu}{\kappa}, \quad Ek = \frac{\nu}{2\Omega H^2}, \quad Ra = \frac{\alpha_T g \Delta H^3}{\nu \kappa}, \tag{2.4}$$

where Γ is the aspect ratio (with L as the horizontal length), Pr is the Prandtl number, Ek is the Ekman number, and Ra is the Rayleigh number, which have been introduced before. The Rossby number $Ro = \sqrt{Ra/Pr}\, Ek$, quantifies the relative strength of buoyancy to the Coriolis force.

The datasets used in this study cover $5 \times 10^{-8} \le Ek \le 5 \times 10^{-6}$, $10^8 \le Ra \le 5 \times 10^{12}$ and $0.125 \le \Gamma \le 2$ for stress-free RRBC, and $5 \times 10^{-9} \le Ek \le 1.5 \times 10^{-8}$, $3 \times 10^{11} \le Ra \le 3 \times 10^{13}$ and $0.125 \le \Gamma \le 0.5$ for no-slip RRBC. All simulations were performed with a fixed Prandtl number $Pr = 1$. Further numerical details can be found in Song *et al.* (2024*c*) for no-slip RRBC, and in Kannan & Zhu (2025) for stress-free RRBC.

We analyse key diagnostic quantities, including Nu and Re, which characterise the vertical momentum transport. These are defined as

$$Nu = 1 + \sqrt{Ra\, Pr}\, \langle u_z \theta \rangle_{V,t}, \quad Re = \sqrt{\frac{Ra}{Pr}} \left\langle u_z^2 \right\rangle_{V,t}^{1/2}, \tag{2.5}$$

where $\langle \cdot \rangle_{V,t}$ denotes averaging over the volume V and time t, and u_z is the non-dimensionalised vertical velocity component.

3. Results and discussion

The Nusselt number Nu is shown in figure 1 as a function of Ra for various Ek values, under both no-slip (red-shaded) and stress-free (blue-shaded) boundary conditions. We observe that for varying control parameters, Nu follows diffusion-free scaling in some regions. Specifically, $Nu - 1 \sim Ra^{3/2}\, Ek^2 \equiv \widetilde{Ra}^{3/2}$, at distinct supercritical Rayleigh numbers $\widetilde{Ra} \equiv Ra\, Ek^{4/3}$, as shown in figure 2(*a*). This diffusion-free scaling holds for moderate values $40 \le \widetilde{Ra} \le 200$ under stress-free conditions, and for higher values $\widetilde{Ra} \ge 200$ under no-slip conditions. Based on the scaling behaviour of Nu, it might be inferred that the whole flow dynamics is diffusion-free.

However, recent work by Song *et al.* (2024*c*) reports that in addition to Nu, both the convective length scale ℓ and the Reynolds number $Re = u_{z,rms} H/\nu$, which characterises momentum transport, also follow diffusion-free scaling in the geostrophic turbulence regime. Here, $u_{z,rms}$ denotes the root mean square (rms) of the vertical velocity component u_z. Specifically, the proposed diffusion-free scaling relations are $\ell/H \sim Ra^{1/2}\, Ek\, Pr^{-1/2}$ and $Re \sim Ra\, Ek\, Pr^{-1}$ (Aurnou *et al.* 2020; Song *et al.* 2024*c*). To explore this further, we examine whether the data obtained under stress-free conditions align with the diffusion-free scaling for ℓ and Re at moderate values of $\widetilde{Ra}$, where Nu exhibits diffusion-free scaling.

The compensated plots for Re and ℓ/H, along with their respective diffusion-free scaling, are presented as functions of $\widetilde{Ra}$ in figures 2(*b*) and 2(*c*). Here, ℓ/H is based on

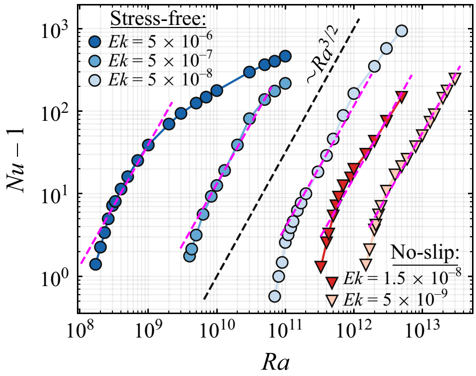

Figure 1. Dimensionless convective heat transport $Nu - 1$ as a function of the Rayleigh number Ra for various Ekman numbers Ek, obtained from DNS of RRBC with stress-free and no-slip boundary conditions at $Pr = 1$. The dashed lines represent the heat transfer scaling for geostrophic turbulence, $Nu - 1 \sim Ra^{3/2}$.

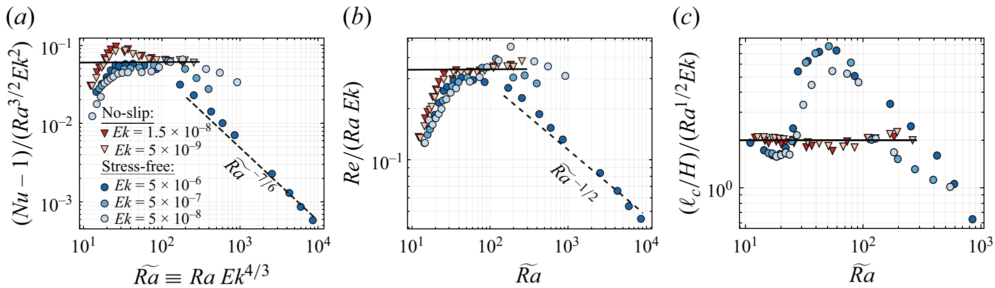

Figure 2. (*a*) Nusselt number $Nu - 1$, normalised by the diffusion-free scaling $Ra^{3/2}\, Ek^2$. (*b*) Dimensionless momentum transport Re, normalised by its geostrophic turbulence scaling $Ra\, Ek$. (*c*) Dimensionless convective length scale ℓ_c/H, normalised by its geostrophic turbulence scaling $Ra^{1/2}\, Ek$, shown as a function of the supercriticality parameter $\widetilde{Ra} \equiv Ra\, Ek^{4/3}$ and increasing supercriticalities.

the u_z spectra, $\ell_c/H = \sum_k [\hat{u}_z(k)\, \hat{u}_z^*(k)] / \sum_k k[\hat{u}_z(k)\, \hat{u}_z^*(k)]$, where $\hat{u}_z(k)$ and $\hat{u}_z^*(k)$ are, respectively, the Fourier transform of u_z and its complex conjugate at the mid-height, and k is the wavenumber. It is evident that at the values of $\widetilde{Ra}$ where Nu follows diffusion-free scaling in figures 1 and 2(*a*), both Re and ℓ_c/H exhibit diffusion-free scaling only under no-slip conditions, as shown by Song *et al.* (2024*c*). However, for stress-free conditions, at moderate values of $40 \leq \widetilde{Ra} \leq 200$, neither Re nor ℓ_c/H data exhibit diffusion-free scaling. This suggests that although the heat transfer is diffusion-free, the momentum transport and associated length still depend on diffusion under the stress-free boundary conditions. Here, it should be noted that the moderate range $40 \leq \widetilde{Ra} \leq 200$ is defined based on our DNS parameters ($Ek \geq 5 \times 10^{-8}$, $Ra \leq 5 \times 10^{12}$). As Ek decreases, the upper bound may increase, potentially broadening the regime where Nu is diffusion-free; however, Re and ℓ/H are not.

This discrepancy raises the question: if Re and ℓ_c/H do not conform to diffusion-free scaling, what alternative scaling do they follow, and how can this behaviour be understood? To address this, we analyse the flow structure to gain insight into the scaling of the associated length scales in this moderate $\widetilde{Ra}$ regime, where heat transfer remains diffusion-free.

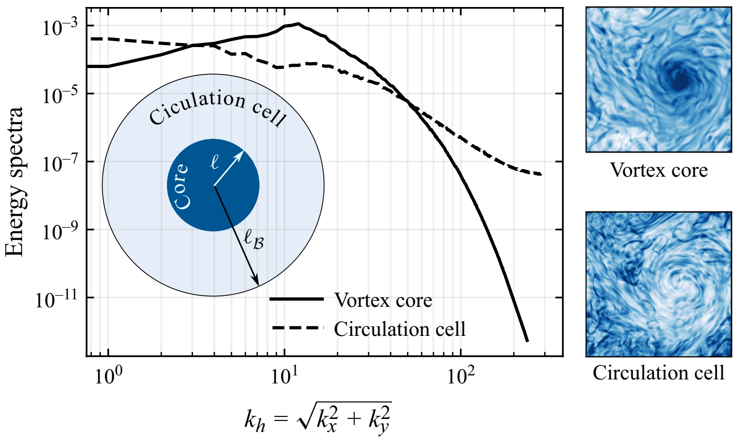

Figure 3. Okubo–Weiss decomposition of barotropic energy at $Ra = 2 \times 10^{11}$, $Ek = 5 \times 10^{-8}$, with spectra for vortex core (solid line) and background circulation cell (dashed line). Vortex core and circulation cell length scales, ℓ and $\ell_{\mathcal{B}}$, are shown in the inset schematic. Right-hand column: contour plots of horizontal vorticity (vortex core) and strain (circulation cell), with dark/light colours for high/low values.

Previous studies for stress-free plates showed that at moderate $\widetilde{Ra}$ values, the flow exhibits a large-scale cyclone–anticyclone vortex dipole with rapidly rotating vortex core (Julien *et al.* 2012*b*; Favier, Silvers & Proctor 2014; Rubio *et al.* 2014; Ecke & Shishkina 2023), a simple structure that fills the domain. For a fixed value of rotation rate (fixed Ek) but increasing Ra, the transport properties trend to those in non-rotating case, i.e. $Nu - 1 \sim Ra^{1/3}$ and $Re \sim Ra^{1/2}$. This behaviour is fully supported by the scalings $(Nu - 1)/(Ra^{3/2}\, Ek^2) \sim Ra^{-7/6}$ and $Re/(Ra\, Ek) \sim Ra^{-1/2}$, as shown in figures 2(*a*) and 2(*b*), respectively.

We now focus on the scaling properties of stress-free flows where the heat transport follows the diffusion-free scaling, i.e. in the range $40 \leq \widetilde{Ra} \leq 200$. They are determined by the scaling relations of the vortex core. To derive them, the large-scale vortex can be viewed spatially as a vortex core (rotation-dominated region) surrounded by a circulation cell (shear-dominated region) in the background, as illustrated in the inset of figure 3 (Petersen, Julien & Weiss 2006). Each circulation cell region has its own length scale: ℓ for the core, and $\ell_{\mathcal{B}}$ for the whole cell.

In the shear-dominated circulation cell, advection is balanced by diffusion across the cell. This region is characterised by slow rotation and dominated by buoyancy forces, unlike the vortex core, which is rotation-dominated. Thus we have the balance

$$\boldsymbol{u} \cdot \boldsymbol{\nabla} \boldsymbol{u} \sim \nu \nabla^2 \boldsymbol{u}. \tag{3.1}$$

In the shear-dominated region of the circulation cell, advective forces locally outweigh the Coriolis effect, despite the system's rapid rotation ($Ek \geq 5 \times 10^{-8}$) – unlike the rotation-dominated vortex core. Thus in the locally buoyancy-dominated region, where rotation is weak, the convective velocity scales with the free-fall velocity u_f, which represents the maximum velocity attainable by a fluid parcel when its potential buoyant energy is fully converted into kinetic energy (Niemela & Sreenivasan 2003; Aurnou *et al.* 2020). This scaling is also supported by our DNS results (see Appendix A). By applying an order-of-magnitude analysis to the above balance, with u_f as the convective velocity scale in the circulation cell, we obtain

$$\frac{u_f^2}{H} \sim \nu \frac{u_f}{\ell_{\mathcal{B}}^2} \implies \frac{\ell_{\mathcal{B}}}{H} \sim Ra^{-1/4}\, Pr^{1/4}. \tag{3.2}$$

For the scales of length in (3.2), the viscous term uses $\ell_{\mathcal{B}}$, the circulation cell's horizontal scale, due to dominant horizontal diffusion, while advection uses H, reflecting vertical momentum transport across the domain.

Similarly, the length scale for the vortex core, which represents the characteristic scale of the flow structure, can be obtained by assuming a balance between viscous and Coriolis forces in the vorticity equation. This assumption is appropriate as the flow in this regime does not follow the diffusion-free scaling for Re and ℓ (see figure 2) deduced from the presumption that the flow obeys a CIA (Coriolis, inertia, Archimedean buoyancy) balance (Aurnou *et al.* 2020; Vasil *et al.* 2021). Therefore, we assume that these structures, particularly the vortex core, are governed by a VAC (viscous, Archimedean buoyancy, Coriolis) balance. The viscous–Coriolis force balance can be written as

$$\nu\, \nabla^2 \boldsymbol{\omega} \sim \varOmega\, \frac{\partial \boldsymbol{u}}{\partial z}, \tag{3.3}$$

where ω is the vorticity field. Here, we consider the length scale in the vortex core, ℓ, to be the diffusion scale that governs the dynamics. We define u as the characteristic velocity scale for the large-scale vortex, and approximate the vorticity of the large-scale roll as $\omega \sim u/\ell_{\mathcal{B}}$. Although the circulation cell is shear-dominated, it shares the same rotational direction as the vortex core and encompasses it, which makes $\ell_{\mathcal{B}}$ an appropriate length scale for estimating the vorticity. In the viscous–Coriolis balance, the Laplacian operates on ℓ, the vortex core's scale – where most dissipation takes place – to balance the Coriolis term ($\varOmega u/H$).

Applying these scaling assumptions, the order-of-magnitude analysis of the above balance yields

$$\frac{\nu}{\ell^2} \frac{u}{\ell_{\mathcal{B}}} \sim \varOmega \frac{u}{H}. \tag{3.4}$$

Substituting the scaling for $\ell_{\mathcal{B}}$ from (3.2) into this relation and rearranging terms, we can express the scaling for the convective length scale ℓ in terms of the control parameters of RRBC as

$$\frac{\ell}{H} \sim Ra^{1/8}\, Pr^{-1/8}\, Ek^{1/2} \equiv \widetilde{Ra}^{1/8}\, Pr^{-1/8}\, Ek^{1/3}. \tag{3.5}$$

The scaling relation $\ell/H \sim Ra^{1/8}$, for fixed Ek and Pr, as presented in (3.5), was also demonstrated by Oliver *et al.* (2023) using asymptotically reduced RRBC simulation data. Through linear stability analysis, Oliver *et al.* (2023) found that the length scale follows $Ra^{1/8}$ scaling, with the most unstable modes growing with Ra as k^{-8}. In contrast, we derive this relation here through force balance and an associated order-of-magnitude analysis.

To compute these two length scales given in (3.2) and (3.5), and verify their scalings for the diffusion-free heat transfer regime, we separate the flow into rotation/vorticity and shear contributions following the Okubo–Weiss decomposition of barotropic (depth-averaged) energy (Okubo 1970; Weiss 1991; Petersen *et al.* 2006; Rubio *et al.* 2014). The corresponding spectra and contour plots for the circulation cell (shear-dominated) and vortex core (rotation-dominated) contributions are shown in figure 3. The dominant length scales for these two regions can be computed individually from these spectra for

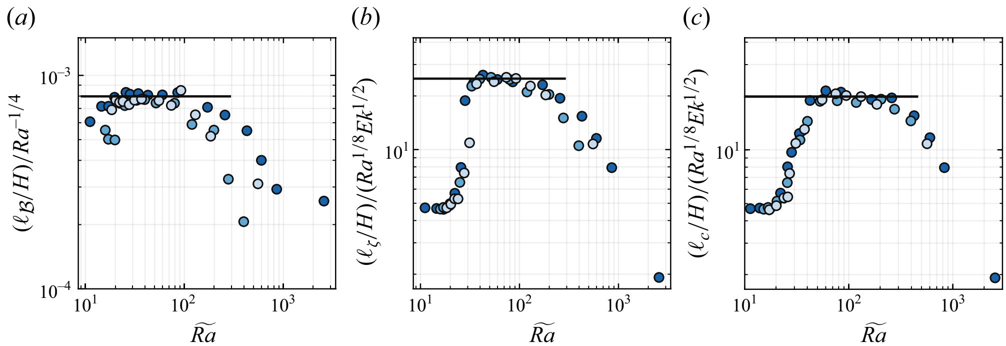

Figure 4. The background convective length scale $\ell_{\mathcal{B}}$, representing the spatial extent of the circulation region. (*b*) The characteristic convective length scale ℓ_ζ, derived from vertical vorticity ω_z. (*c*) The convective length scale ℓ_c, based on vertical velocity. All are normalised by the new scaling laws proposed in (3.2) and (3.5), within the diffusion-free heat transfer regime. These are plotted as functions of $\widetilde{Ra} = Ra\, Ek^{4/3}$. A power-law fit to the DNS data in the moderate range $40 \le \widetilde{Ra} \le 200$ yields the scaling relation $Re \sim \widetilde{Ra}^{\alpha}$ at fixed Ek, with fitted exponents α for (*a*) $\ell/H = 0.23 \pm 0.12$, (*b*) $\ell_\zeta/H = 0.11 \pm 0.09$ and (*c*) $\ell_c/H = 0.12 \pm 0.05$ (95 % confidence interval), supporting the scaling relations presented in (3.2) and (3.5).

different cases. The length scales $\ell_{\mathcal{B}}$, derived from shear spectra, and ℓ, computed from depth-averaged vertical vorticity spectra, and denoted as ℓ_ζ to represent the rotational contribution, are plotted as functions of $\widetilde{Ra}$ in figures 4(*a*) and 4(*b*), respectively. It can be seen that at moderate $40 \le \widetilde{Ra} \le 200$ in the diffusion-free heat transfer regime, the scalings deduced in (3.2) and (3.5) show good agreement. The scales $\ell_{\mathcal{B}}$ and ℓ reflect the dipole's multi-scale dynamics, yielding (3.5), which agrees with the DNS data (figure 4), thereby confirming the validity of these scale choices. The scaling $\ell/H \sim \widetilde{Ra}^{1/8}\, Ek^{1/3}$ holds approximately in $40 \le \widetilde{Ra} \le 200$, with figure 4(*a*) showing validity from $\widetilde{Ra} \approx 20$ to $\sim$100, and figures 4(*b*,*c*) extending to ~ 200. Deviations reflect evolving flow structures at higher $\widetilde{Ra}$ on decreasing Ek. The convective length scale can be determined from temperature, vertical velocity and vertical vorticity, as the spatial correlations of these quantities are qualitatively similar across the cell, columns, plumes and geostrophic turbulence regimes (Nieves, Rubio & Julien 2014). Notably, the convective length scale calculated from vertical velocity ℓ_c, as in figure 2(*c*), aligns well with the deduced scaling in (3.5) for moderate $\widetilde{Ra}$ values (see figure 4*c*).

Having established the convective length scale, we now focus on obtaining the scaling for momentum transport, characterised by Re, in the diffusion-free heat transfer regime. To determine the scaling of Re, we follow the approach outlined by Song *et al.* (2024*c*), where it was derived using exact relations that Nu and Re are related to ℓ by the equation

$$Re \sim \frac{Nu - 1}{(\ell/H)\ Pr} \tag{3.6}$$

in this regime. Substituting $Nu - 1 \sim Ra^{3/2}\, Pr^{-1/2}\, Ek^2$ and $\ell/H \sim Ra^{1/8}\, Pr^{-1/8}\, Ek^{1/2}$ from (3.5) into this relation, we obtain the scaling for Re in the moderate $\widetilde{Ra}$ diffusion-free heat transfer regime:

$$Re \sim Ra^{11/8}\, Pr^{-11/8}\, Ek^{3/2} \equiv \widetilde{Ra}^{11/8}\, Pr^{-11/8}\, Ek^{-1/3}. \tag{3.7}$$

The above scaling was also recently derived by Kannan & Zhu (2025) using the transition Rayleigh number scaling for stress-free RRBC, $Ra_T \sim Ek^{-12/7}$, which marks

https://doi.org/10.1017/jfm.2025.10384 Published online by Cambridge University Press

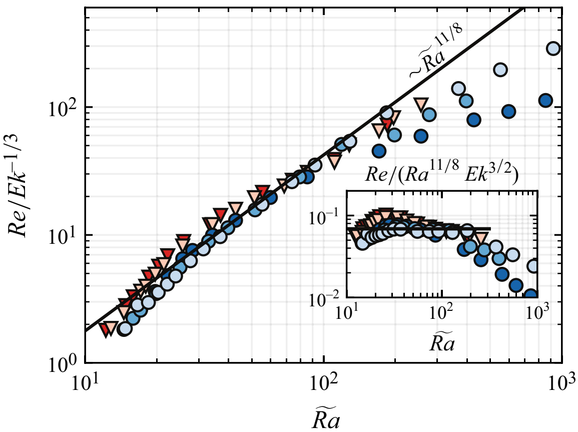

Figure 5. Dimensionless momentum transport Re, normalised by $Ek^{-1/3}$, versus supercriticality $\widetilde{Ra} = Ra\,Ek^{4/3}$ for stress-free (circles) and no-slip (triangles) RRBC. Inset: Re, normalised by (3.7), in the diffusion-free heat transfer regime, versus $\widetilde{Ra}$. A power-law fit to stress-free DNS data for $40 \le \widetilde{Ra} \le 200$ gives $Re \sim \widetilde{Ra}^{\alpha}$ at fixed Ek, with $\alpha = 1.26 \pm 0.14$ (95 % confidence interval), which supports (3.7) and which is clearly different from the diffusion-free scaling for no-slip boundary condition as shown in figure 2(*b*).

the shift from rotation- to buoyancy-dominated regimes. For stress-free RRBC in the rotation-dominated regime at fixed $Pr = 1$, the scaling $Re \sim Ra^{11/8}\,Ek^{3/2}$ is obtained by equating the buoyancy-dominated scaling $Re \sim Ra^{1/2}$ with Ra_T. Additionally, numerical simulations by Oliver *et al.* (2023), using an asymptotically reduced model, report $Re \sim Ra^{1.325}$ from an empirical fit for $40 \le \widetilde{Ra} \le 200$. This exponent closely matches the theoretical $11/8 = 1.375$ scaling derived here (3.7) for moderate $\widetilde{Ra}$.

Figure 5 shows a compensated plot of Re versus $\widetilde{Ra}$, where Re is normalised by the scaling in (3.7), for the diffusion-free heat transfer regime in stress-free and no-slip RRBC. The plot confirms that Re follows the predicted scaling for stress-free RRBC in this regime of moderate $\widetilde{Ra}$, and clearly deviates for no-slip RRBC .

Although the range of Ra over which Nu follows the diffusion-free scaling increases with decreasing Ek (as seen in figures 1 and 2*a*), the length scales ℓ_ζ and ℓ_c do not exhibit a similar broadening in figures 4(*b*) and 4(*c*). This difference arises because ℓ reflects finer structural features of the flow, such as the presence and breakdown of coherent vortices, which evolve non-monotonically with control parameters. Therefore, asymptotic scaling in ℓ may require even lower Ek to emerge clearly. Meanwhile, the derived scaling for Re appears valid over a broader range at low Ek (see figure 5), partly because Re depends analytically on Nu and ℓ, and inherits smoothness from the former.

These results indicate that while Nu follows diffusion-free scaling under specific flow parameters for stress-free conditions, the corresponding scalings for ℓ and Re can remain highly dependent on molecular diffusivity (see (3.5) and (3.7)). Therefore, for the flow to be considered truly diffusion-free, both convective and momentum transport, along with their associated length scales, must be independent of molecular diffusivity.

4. Conclusions

This study investigated the scaling behaviour of the Nusselt number (Nu), Reynolds number (Re) and convective length scale (ℓ) in RRBC with stress-free boundaries, using our available DNS data. While Nu followed diffusion-free scaling for some parameter

https://doi.org/10.1017/jfm.2025.10384 Published online by Cambridge University Press

range, Re and ℓ did not, revealing that Nu scaling alone cannot guarantee geostrophic turbulence. Therefore, the Pr dependence reported in this study should be interpreted with caution and still requires further validation. We proposed new scaling relations for Re and ℓ in this diffusion-free heat transfer regime, showing that an accurate assessment of both thermal and dynamic properties is essential to characterise geostrophic turbulence accurately in stress-free conditions. These findings suggest that achieving fully diffusion-free turbulence in DNS may require more extreme rotational conditions than previously expected. Extrapolating our scalings suggests diffusion-free behaviour at $Ek \sim Ra^{-1/4}$ (e.g. $Ek \sim 10^{-9}$ for $Ra \sim 10^{12}$ at $Pr = 1$), requiring smaller Ekman numbers than those studied here, consistent with results from van Kan *et al.* (2025) using a rescaled RRBC model. By emphasising the importance of boundary conditions and multi-parameter scaling, this work advances understanding of RRBC in geophysical and astrophysical contexts, and encourages further research on geostrophic turbulence.

Our scaling laws can be compared to theoretical bounds derived by Tilgner (2022), who investigated upper limits on heat transfer and kinetic energy in RRBC with stress-free boundaries at large Prandtl numbers. These bounds, derived via a variational approach, suggest that Nu scales at most as $Nu \sim Ra$ in the infinite Pr limit, moderated by rotational effects, while kinetic energy constraints reflect a balance between viscous dissipation and Coriolis forces. In our moderate Prandtl number regime ($Pr = 1$, moderate $\widetilde{Ra}$), Nu aligns with the diffusion-free scaling $Nu - 1 \sim Ra^{3/2}\, Ek^2$, which exceeds Tilgner's bound at lower Ra but may approach consistency at higher Ra as rotational suppression intensifies. Meanwhile, our Re scaling ($Re \sim Ra^{11/8}\, Ek^{3/2}$) indicates a stronger Ra dependence, which might be constrained by kinetic energy bounds at infinite Pr, highlighting the influence of finite Prandtl number effects in our DNS data. This comparison underscores the need for further exploration of Prandtl number dependencies to reconcile empirical scalings with theoretical maxima.

Funding. We gratefully acknowledge financial support from the Max Planck Society and the German Research Foundation through grants 521319293, 540422505 and 550262949. All the simulations have been conducted on the HPC systems of the Max Planck Computing and Data Facility (MPCDF) as well as the National High Performance Computing (NHR@ZIB and NHR-Nord@Göttingen).

Declaration of interests. The authors report no conflict of interest.

Appendix A. Velocity scale in the circulation cell

Figure 6 shows vertical velocity u_z and streamfunction ψ contours at mid-plane for a cyclonic vortex at $Ra = 2 \times 10^{11}$, $Ek = 5 \times 10^{-8}$, $Pr = 1$ ($\tilde{Ra} \approx 126$), with a fast-rotating core in a circulation cell (see inset) (Petersen *et al.* 2006). The dipole, with a dominant cyclonic vortex, aligns with dipolar structures in the literature (Julien *et al.* 2012*b*; Rubio *et al.* 2014). The cell's convective velocity $u_{z,cell}$, averaged where $|\psi| \leq 0.8\, |\psi|\mathrm{max}$, yields $Re_{z,cell} = u_{z,cell,rms} H/\nu$, plotted versus $Ra^{1/2}$ in figure 6. We find $Re_{z,cell} \sim Ra^{1/2}$, matching u_f scaling from buoyancy-dominated regimes (Niemela & Sreenivasan 2003; Aurnou *et al.* 2020), which informs the length scale $\ell_{\mathcal{B}}$ in (3.2). Within the shear-dominated circulation cell, where rotational effects are minimal, buoyancy drives the flow, and the convective velocity scales as the free-fall velocity, yielding $Re_{z,cell} \sim Ra^{1/2}$. This localised scaling reflects the dominance of buoyancy in this region, contrasting with the rotationally influenced three-dimensional dynamics of the broader flow, including the vortex core.

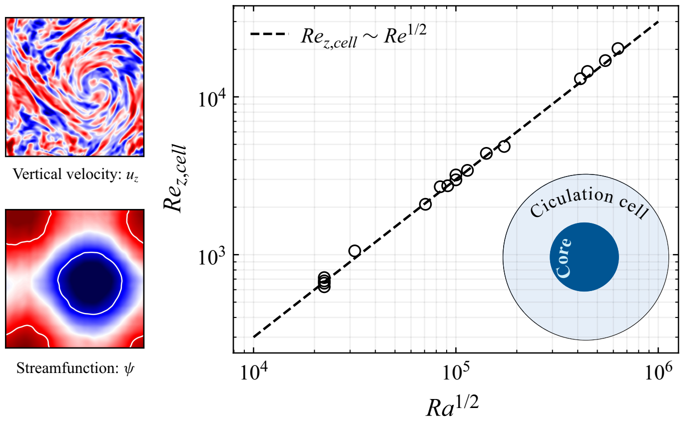

Figure 6. Left-hand column: instantaneous u_z and ψ contours at mid-plane for a large-scale vortex at $Ra = 2 \times 10^{11}$, $Pr = 1$, $Ek = 5 \times 10^{-8}$ (red/blue for positive/negative values; white line at $\psi = 0.8\psi_{max}$ marks vortex core). Right-hand column: $Re_{z,cell}$ in the circulation cell ($|\psi| \leq 0.8\psi_{max}$) versus $Ra^{1/2}$. Inset: schematic of vortex core and circulation cell.

REFERENCES

AHLERS, G., GROSSMANN, S. & LOHSE, D. 2009 Heat transfer and large scale dynamics in turbulent Rayleigh–Bénard convection. *Rev. Mod. Phys.* **81** (2), 503–537.

ATKINSON, B.W. & ZHANG, J.W. 1996 Mesoscale shallow convection in the atmosphere. *Rev. Geophys.* **34** (4), 403–431.

AURNOU, J.M., CALKINS, M.A., CHENG, J.S., JULIEN, K., KING, E.M., NIEVES, D., SODERLUND, K.M. & STELLMACH, S. 2015 Rotating convective turbulence in Earth and planetary cores. *Phys. Earth Planet. Inter.* **246**, 52–71.

AURNOU, J.M., HORN, S. & JULIEN, K. 2020 Connections between nonrotating, slowly rotating, and rapidly rotating turbulent convection transport scalings. *Phys. Rev. Res.* **2** (4), 043115.

BOUILLAUT, V., MIQUEL, B., JULIEN, K., AUMAÎTRE, S. & GALLET, B. 2021 Experimental observation of the geostrophic turbulence regime of rapidly rotating convection. *Proc. Natl Acad. Sci. USA* **118** (44), e2105015118.

CHENG, J.S. & AURNOU, J.M. 2016 Tests of diffusion-free scaling behaviors in numerical dynamo datasets. *Earth Planet. Sci. Lett.* **436**, 121–129.

CHENG, J.S., AURNOU, J.M., JULIEN, K. & KUNNEN, R.P.J. 2018 A heuristic framework for next-generation models of geostrophic convective turbulence. *Geophys. Astrophys. Fluid Dyn.* **112** (4), 277–300.

CHENG, J.S., STELLMACH, S., RIBEIRO, A., GRANNAN, A., KING, E.M. & AURNOU, J.M. 2015 Laboratory-numerical models of rapidly rotating convection in planetary cores. *Geophys. J. Intl* **201** (1), 1–17.

CHRISTENSEN, U.R. 2010 Dynamo scaling laws and applications to the planets. *Space Sci. Rev.* **152** (1–4), 565–590.

ECKE, R.E. & SHISHKINA, O. 2023 Turbulent rotating Rayleigh–Bénard convection. *Annu. Rev. Fluid Mech.* **55** (1), 603–638.

FAVIER, B., SILVERS, L.J. & PROCTOR, M.R.E. 2014 Inverse cascade and symmetry breaking in rapidly rotating Boussinesq convection. *Phys. Fluids* **26** (9), 096605.

FEATHERSTONE, N.A. & HINDMAN, B.W. 2016 The emergence of solar supergranulation as a natural consequence of rotationally constrained interior convection. *Astrophys. J. Lett.* **830** (1), L15.

FUENTES, J.R., ANDERS, E.H., CUMMING, A. & HINDMAN, B.W. 2023 Rotation reduces convective mixing in Jupiter and other gas giants. *Astrophys. J. Lett.* **950** (1), L4.

GUERVILLY, C., CARDIN, P. & SCHAEFFER, N. 2019 Turbulent convective length scale in planetary cores. *Nature* **570** (7761), 368–371.

HEIMPEL, M., GASTINE, T. & WICHT, J. 2016 Simulation of deep-seated zonal jets and shallow vortices in gas giant atmospheres. *Nat. Geosci.* **9** (1), 19–23.

JULIEN, K., KNOBLOCH, E., RUBIO, A.M. & VASIL, G.M. 2012*a* Heat transport in low-Rossby-number Rayleigh–Bénard convection. *Phys. Rev. Lett.* **109** (25), 254503.

JULIEN, K., RUBIO, A.M., GROOMS, I. & KNOBLOCH, E. 2012*b* Statistical and physical balances in low Rossby number Rayleigh–Bénard convection. *Geophys. Astrophys. Fluid Dyn.* **106** (4–5), 392–428.

VAN KAN, A., JULIEN, K., MIQUEL, B. & KNOBLOCH, E. 2025 Bridging the Rossby number gap in rapidly rotating thermal convection. *J. Fluid Mech.* **1010**, A42.

KANNAN, V. & ZHU, X. 2025 Transition between rotation- and buoyancy-dominated regimes in rotating convection: the effect of boundary conditions. *J. Fluid Mech.* **1011**, A7.

KÄPYLÄ, P.J. 2024 Convective scale and subadiabatic layers in simulations of rotating compressible convection. *Astron. Astrophys.* **683**, A221.

KUNNEN, R.P.J. 2021 The geostrophic regime of rapidly rotating turbulent convection. *J. Turbul.* **22** (4–5), 267–296.

LOHSE, D. & SHISHKINA, O. 2024 Ultimate Rayleigh–Bénard turbulence. *Rev. Mod. Phys.* **96** (3), 035001.

MADONIA, M., AGUIRRE GUZMÁN, A.J., CLERCX, H.J.H. & KUNNEN, R.P.J. 2021 Velocimetry in rapidly rotating convection: spatial correlations, flow structures and length scales. *Europhys. Lett.* **135** (5), 54002.

MAFFEI, S., KROUSS, M.J., JULIEN, K. & CALKINS, M.A. 2021 On the inverse cascade and flow speed scaling behaviour in rapidly rotating Rayleigh–Bénard convection. *J. Fluid Mech.* **913**, A18.

MARSHALL, J. & SCHOTT, F. 1999 Open-ocean convection: observations, theory, and models. *Rev. Geophys.* **37** (1), 1–64.

NIEMELA, J.J. & SREENIVASAN, K.R. 2003 Rayleigh-number evolution of large-scale coherent motion in turbulent convection. *Europhys. Lett.* **62** (6), 829–833.

NIEVES, D., RUBIO, A.M. & JULIEN, K. 2014 Statistical classification of flow morphology in rapidly rotating Rayleigh–Bénard convection. *Phys. Fluids* **26** (8), 086602.

OKUBO, A. 1970 Horizontal dispersion of floatable particles in the vicinity of velocity singularities such as convergences. *Deep Sea Res.* **17**, 445–454.

OLIVER, T.G., JACOBI, A.S., JULIEN, K. & CALKINS, M.A. 2023 Small scale quasigeostrophic convective turbulence at large Rayleigh number. *Phys. Rev. Fluids* **8** (9), 093502.

PETERSEN, M.R., JULIEN, K. & WEISS, J.B. 2006 Vortex cores, strain cells, and filaments in quasigeostrophic turbulence. *Phys. Fluids* **18** (2), 026601.

PLUMLEY, M. & JULIEN, K. 2019 Scaling laws in Rayleigh–Bénard convection. *Earth Space Sci.* **34** (9), 1580–1592.

PLUMLEY, M., JULIEN, K., MARTI, P. & STELLMACH, S. 2017 Sensitivity of rapidly rotating Rayleigh–Bénard convection to Ekman pumping. *Phys. Rev. Fluids* **2** (9), 094801.

VAN DER POEL, E.P., OSTILLA-MÓNICO, R., DONNERS, J. & VERZICCO, R. 2015 A pencil distributed finite difference code for strongly turbulent wall–bounded flows. *Comput. Fluids* **116**, 10–16.

RUBIO, A.M., JULIEN, K., KNOBLOCH, E. & WEISS, J.B. 2014 Upscale energy transfer in three-dimensional rapidly rotating turbulent convection. *Phys. Rev. Lett.* **112** (14), 144501.

SCHUMACHER, J. & SREENIVASAN, K.R. 2020 Colloquium: unusual dynamics of convection in the sun. *Rev. Mod. Phys.* **92** (4), 041001.

SONG, J., KANNAN, V., SHISHKINA, O. & ZHU, X. 2024*a* Direct numerical simulations of the transition between rotation- to buoyancy-dominated regimes in rotating Rayleigh–Bénard convection. *Intl J. Heat Mass Transfer* **232**, 125971.

SONG, J., SHISHKINA, O. & ZHU, X. 2024*b* Direct numerical simulations of rapidly rotating Rayleigh–Bénard convection with Rayleigh number up to 5×10^{13}. *J. Fluid Mech.* **989**, A3.

SONG, J., SHISHKINA, O. & ZHU, X. 2024*c* Scaling regimes in rapidly rotating thermal convection at extreme Rayleigh numbers. *J. Fluid Mech.* **984**, A45.

STELLMACH, S., LISCHPER, M., JULIEN, K., VASIL, G., CHENG, J.S., RIBEIRO, A., KING, E.M. & AURNOU, J.M. 2014 Approaching the asymptotic regime of rapidly rotating convection: boundary layers versus interior dynamics. *Phys. Rev. Lett.* **113** (25), 254501.

STEVENSON, D.J. 1979 Turbulent thermal convection in the presence of rotation and a magnetic field – a heuristic theory. *Geophys. Astrophys. Fluid Dyn.* **12** (1), 139–169.

TILGNER, A. 2022 Bounds for rotating Rayleigh–Bénard convection at large Prandtl number. *J. Fluid Mech.* **930**, A33.

VALLIS, G.K. 2017 *Atmospheric and Oceanic Fluid Dynamics*. Cambridge University Press.

VASIL, G.M., JULIEN, K. & FEATHERSTONE, N.A. 2021 Rotation suppresses giant-scale solar convection. *Proc. Natl Acad. Sci. USA* **118** (31), e2022518118.

VERZICCO, R. & ORLANDI, P. 1996 A finite-difference scheme for three-dimensional incompressible flow in cylindrical coordinates. *J. Comput. Phys.* **123** (2), 402–413.

WEISS, J. 1991 The dynamics of enstrophy transfer in two-dimensional hydrodynamics. *Physica D* **48** (2–3), 273–294.

ZHU, X. 2018 AFiD-GPU: a versatile Navier–Stokes solver for wall-bounded turbulent flows on GPU clusters. *Comput. Phys. Commun.* **229**, 199–210.